JACS
JOURNAL OF THE AMERICAN CHEMICAL SOCIETY

Article

pubs.acs.org/JACS

Protein Adsorption and Reorganization on Nanoparticles Probed by the Coffee-Ring Effect: Application to Single Point Mutation Detection

Stéphanie Devineau,[†,‡,⊥] Manos Anyfantakis,[†,‡] Laurent Marichal,[§] Laurent Kiger,[∥] Mathieu Morel,[†,‡] Sergii Rudiuk,[†,‡] and Damien Baigl*[,†,‡]

[†]Ecole normale supérieure, PSL Research University, UPMC Univ Paris 06, CNRS, Department of Chemistry, PASTEUR, 24 rue Lhomond, 75005 Paris, France

[‡]Sorbonne Universités, UPMC Univ Paris 06, ENS, CNRS, PASTEUR, 75005 Paris, France

[§]LIONS, NIMBE, CEA, CNRS, Université Paris-Saclay, CEA Saclay, 91191 Gif sur Yvette, France

[∥]IMRB-INSERM U955, 5 rue Gustave Eiffel, 94017 Creteil Cedex, France

Supporting Information

ABSTRACT: The coffee-ring effect denotes the accumulation of particles at the edge of an evaporating sessile drop pinned on a substrate. Because it can be detected by simple visual inspection, this ubiquitous phenomenon can be envisioned as a robust and cost-effective diagnostic tool. Toward this direction, here we systematically analyze the deposit morphology of drying drops containing polystyrene particles of different surface properties with various proteins (bovine serum albumin (BSA) and different forms of hemoglobin). We show that deposit patterns reveal information on both the adsorption of proteins onto particles and their reorganization following adsorption. By combining pattern analysis with adsorption isotherm and zeta potential measurements, we show that the suppression of the coffee-ring effect and the formation of a disk-shaped pattern is primarily associated with particle neutralization by protein adsorption. However, our findings also suggest that protein reorganization following adsorption can dramatically invert this tendency. Exposure of hydrophobic (respectively charged) residues can lead to disk (respectively ring) deposit morphologies independently of the global particle charge. Surface tension measurements and microscopic observations of the evaporating drops show that the determinant factor of the deposit morphology is the accumulation of particles at the liquid/gas interface during evaporation. This general behavior opens the possibility to probe protein adsorption and reorganization on particles by the analysis of the deposit patterns, the formation of a disk being the robust signature of particles rendered hydrophobic by protein adsorption. We show that this method is sensitive enough to detect a single point mutation in a protein, as demonstrated here by the distinct patterns formed by human native hemoglobin h-HbA and its mutant form h-HbS, which is responsible for sickle cell anemia.

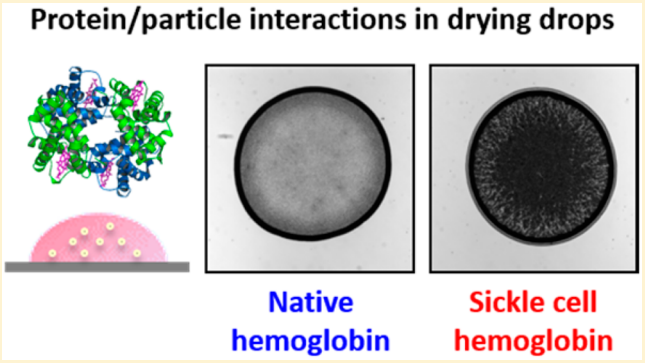

INTRODUCTION

The coffee-ring effect (CRE) describes the deposition of particles at the edge of a drop during drying of a colloidal suspension, as one can observe in the black ring of a coffee stain. The physics of the CRE was first explained by Deegan et al.[1] When a drop is pinned on a substrate, the higher evaporation rate at the contact line induces a strong capillary flow that thoroughly transports particles from the bulk to the contact line where they accumulate. The CRE is a phenomenon that can occur with any drying drop containing nonvolatile solutes, including not only inert particles but also biological entities such as bacteria,[2,3] viruses[4] and proteins.[5−7] This ubiquitous character makes the occurrence of the CRE an obstacle in many types of applications ranging from inkjet printing[8] to DNA microarrays,[9,10] protein microarrays[11−13] and cell patterning.[14] Much effort has thus been devoted to control or suppress the CRE. Successful strategies have usually relied on affecting either one of the two key components at the origin of the CRE, i.e., the capillary flow toward the edge of the drop and the pinning of the contact line, or by tuning interactions between particles and interfaces.[15−18] This implied the use of additives such as surfactants,[19,20] polymers,[21] sol−gel inducers[22] and cosolvents,[8] or the application of electric[23] or optical[24,25] stimulations. However, how proteins can affect the deposition behavior of particles in an evaporating drop remains largely

Received: May 10, 2016
Published: August 25, 2016

DOI: 10.1021/jacs.6b04833
J. Am. Chem. Soc. 2016, 138, 11623−11632

unknown. Knowing that both synthetic polymers and surfactants can affect the CRE, one can raise the question whether adding biomolecules such as proteins to a particle suspension would change the pattern formation upon drop drying and, if so, what distinguishes proteins from ordinary polymers and surfactants.

Moreover, the CRE can be seen as a tool to be exploited.[18] First, the accumulation of particles at specific locations inside a drying drop has been used for particle patterning on surfaces.[25−27] Interestingly, such accumulation effects were also exploited in diagnostic assays to enhance the sensitivity of biomarker detection at the ring position.[28,29] The direct analysis of the pattern morphology to extract information on interactions occurring in a drying drop has also been exploited in a few notable cases. The strategy has always consisted in using particles with a specific surface modification, such as Ni(II)NTA ligands,[30] streptavidin/biotin,[31] antibodies[32] or oligonucleotides.[33] In the presence of the target, particles usually aggregated resulting in the suppression of the CRE[33] or in the change of the deposit size.[32] All of these methods relied on specific formulations with particles designed to aggregate in the presence of a predefined target. By contrast, the general effects of proteins on the drying behavior of drops containing conventional particles have never been investigated. It is well-known that many proteins can nonspecifically interact with particles by adsorption, through electrostatic or hydrophobic interactions.[34−36] We thus hypothesized that analyzing the patterns of drying drops containing different types of particles and proteins would not only reveal information on protein/particle interactions but would also bring valuable insight for the current development of cost-effective CRE-based diagnostic assays.

In this paper, we investigated the relationship between protein/particle interactions and pattern formation in drying drops in a systematic way for the first time. We used 500 nm diameter polystyrene particles with various surface functionalities. We first analyzed the effect of two model proteins, bovine serum albumin (BSA) and porcine hemoglobin (p-HbA) on the deposit patterns of the particles. To better understand the effect of protein/particle interaction, we systematically studied the adsorption behavior of the proteins on the different particles and analyzed the effect of both electrostatic and hydrophobic interactions on the deposit patterns. Notably, this allowed us to extract the first general rules linking the pattern morphology to both protein adsorption and reorganization behavior on nanoparticle surfaces. This novel fundamental knowledge was finally applied to detect a single point mutation in a human protein. For instance, we established conditions for which deposit patterns revealed whether the human hemoglobin initially in the drop was in its native healthy form (h-HbA) or in its mutant, pathogenic form (h-HbS) responsible for sickle cell anemia, a major blood genetic disease.

EXPERIMENTAL SECTION

Proteins. Human adult hemoglobin, in both native (h-HbA) and mutant (h-HBS) forms, was purified from fresh donor blood following standard preparation[37] and dialyzed against pure water at 4 °C overnight. h-HbA and h-HbS in the oxygenated form were aliquoted and stored at −80 °C. Porcine HbA (p-HbA) was purified following the same protocol and was used as fresh solution only. Lyophilized bovine serum albumin (Sigma, A0281) and metmyoglobin (Mb) from equine heart (Sigma, M1882) were dissolved and dialyzed in pure water. All the protein solutions were centrifuged at 14 000*g* for 5 min at 4 °C before use. Protein concentrations were measured on a Shimadzu UV-2450 spectrophotometer.[38,39] Hemoglobin integrity was checked by measuring the absorption coefficient ratio $\varepsilon_{576}/\varepsilon_{541}$ indicative of iron oxidation and protein damage.[40] Hemoglobin concentration is expressed as heme molar concentration.

Polystyrene Particles. The cationic polystyrene particles with amidine surface groups (PS-AMI, 510 ± 23 nm in diameter, cat. no. A37317), the anionic polystyrene particles with sulfate surface groups (PS-SU, 510 ± 32 nm in diameter, cat. no. S37494) and with carboxylate surface groups (PS-CA, 450 ± 5 nm in diameter, cat. no. C37269) were purchased from Life technologies.

Deposit Patterns. All the solutions were prepared in ultrapure water (18.2 MΩ·cm). The particle suspension was diluted in water, sonicated for 1 min and vortexed before addition of protein to give a final volume of 50 μL with a particle concentration of 2 mg/mL. The sample was then gently mixed for 30 min at room temperature before deposition with a micropipette of a 0.8 μL droplet on a glass coverslip (Menzel−Gläser) used as received. The contact angle of pure water droplets on the glass substrate was previously measured to be $\theta = 55 \pm 2°$ indicating partial wetting.[20] The drops were protected from air flows during drying by a cover. Drying conditions were 23 ± 1 °C and 35−55% relative humidity. Deposit patterns were imaged in a brightfield transmission mode with an inverted optical microscope (Zeiss Axio Observer) equipped with an EMCCD camera (Photometrics CoolSNAP HQ2 or Photometrics CoolSNAP MYO, Princeton Instruments). Images were acquired in similar illumination conditions and are displayed without further processing. Each experiment was repeated three times.

Surface Tension Measurements. Surface tension was measured on a DSA30 Drop Shape Analysis System (Krüss). The surface tension was determined by fitting the shape of a ∼10 μL pendant drop with the Young−Laplace equation. Each measurement was repeated 3 times.

Deposit Pattern Analysis. Quantitative analysis of the deposition patterns was carried out using ImageJ software. The image of the deposit was first normalized by a blank image taken under the same conditions without deposit. The radial intensity profile of each deposit pattern was then automatically extracted starting from the center of each drop. The average intensity in the 0−70% inner area of the drop (I_1) and the minimum intensity corresponding to particle deposition in the ring (I_2) were extracted to calculate the Ring Factor (RF) as follow $RF = I_1 - I_2$.[24]

Adsorption Isotherms. Adsorption isotherms of proteins on PS particles were measured by the depletion method. Protein solution was added to the particle suspension with a final particle concentration of 6 mg/mL prior to gentle mixing for 3 h at 20 °C. The sample was then centrifuged at 30 000*g* for 1 h. The supernatant was carefully removed and centrifuged again at 30 000*g* for 30 min. The protein concentration in the supernatant was measured at the Soret band for p-HbA ($\varepsilon_{414nm} = 1.3 \times 10^5$ M^{-1} cm^{-1}) and Mb ($\varepsilon_{409nm} = 1.89 \times 10^5$ M^{-1} cm^{-1}) to enhance sensitivity at low protein concentration. An uncertainty of 0.2 mg/m^2 on the amount of adsorbed protein was achieved by repeating 5 times this procedure.

Zeta Potential and pH Measurement. Zeta potential (ζ) of PS particles was measured on a Zetasizer Nano-ZS (Malvern Instruments) at 20 °C. Due to strong scattering of the original suspensions, samples prepared for drying drop experiments were diluted 10 times in pure water before the measurement leading to a final particle concentration of 0.2 mg/mL and a 10-fold decrease of protein concentration. Each measurement was repeated three times. The zeta potential was calculated by fitting the electrophoretic mobility with the Smoluchowski model and averaged over three different samples. ζ was plotted as a function of an equivalent protein concentration, which corresponded to the protein concentration in the protein/particle mixture before dilution (see Figures 4B, 6B, 7). The pH was measured at 20 °C with a Mettler Toledo S 220 pH meter and an InLab Nano electrode.

DOI: 10.1021/jacs.6b04833
J. Am. Chem. Soc. 2016, 138, 11623−11632

RESULTS AND DISCUSSION

Particles of similar sizes (around 500 nm in diameter) and density (polystyrene core) but different charges were mixed at a fixed concentration (2 mg/mL) with increasing concentrations of purified proteins (Figure 1A). We first used two model

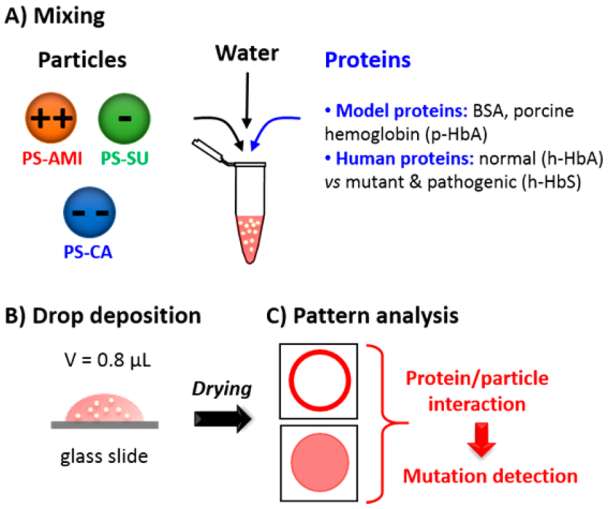

Figure 1. Protein/particle interactions probed by the coffee-ring effect. (A) A solution is obtained by mixing water, functionalized polystyrene particles (about 500 nm in diameter) at a fixed concentration (2 mg/mL), and proteins at various concentrations. Particles are highly cationic (PS-AMI), anionic (PS-SU), or highly anionic (PS-CA). Proteins are bovine serum albumin (BSA), porcine hemoglobin (p-HbA), and human hemoglobin in native (h-HbA) or mutant (h-HbS) form. (B) A 0.8 μL drop is deposited on a glass slide. (C) After drying, the pattern analysis provides fundamental information on protein/particle interactions (protein adsorption and reorganization). The method is applied to the detection of a pathogenic, single-point mutation in hemoglobin.

proteins, bovine serum albumin (BSA) and porcine hemoglobin (p-HbA), to extract general information linking protein/particle interaction and pattern morphology after drop drying, prior to applying this method to the detection of a pathogenic single-point mutation in a human protein (Figure 1B,C).

Effect of BSA on the Deposit Patterns of PS Particles. We started by investigating the effect of BSA, a negatively charged protein in pure water (isoelectric point IEP pH ~ 4.8), on the deposit patterns of PS particles as a function of particle charge and protein concentration (Figures 2, S1–S3).

In the case of anionic particles (PS-SU and PS-CA) and in the absence of proteins (Figure 2, top row), a marked black ring was formed, in agreement with the conventional CRE where particles accumulated near the contact line due to the outward evaporation-driven capillary flow. For these particles, the addition of BSA had no major influence on the evolution of the particle pattern and the black ring of particles was observed for BSA concentrations ranging from 0 to 34 μM (Figure 2 *middle* and *right*, Figures S1–S2). For low BSA concentrations (<5 μM), the presence of the protein in the deposit was hardly distinguished. In contrast, for [BSA] $\geq$ 5 μM, one or several light-gray rings surrounding the black particle ring were reproducibly observed. Control experiments in the absence of particles at various BSA concentrations (Figure S4) clearly indicated that these gray rings corresponded to proteins accumulated at the outer edge of the deposit. The formation of protein rings in drying drops was reported by other groups

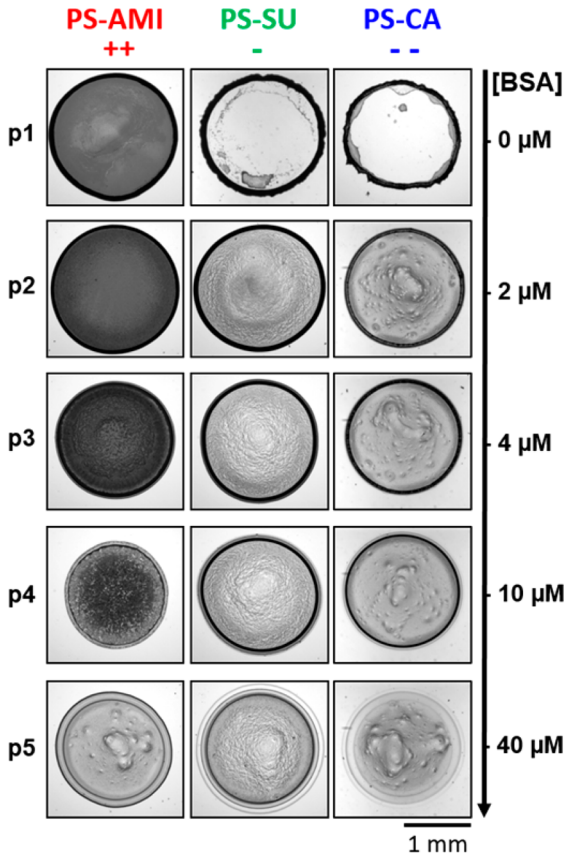

Figure 2. Effect of BSA on deposit morphologies. Representative brightfield microscope images of the deposit patterns obtained with PS-AMI (left), PS-SU (middle), and PS-CA (right) as a function of BSA concentration. The pattern names, p1–p5, which refer to each BSA concentration, are those used in Figure 4B.

for various purified proteins[5,6,41] but, to our knowledge, it is the first time that protein rings surrounding particle rings in drop deposits are reported. A multiple-ring pattern is usually associated with the sorting of particles of different sizes during drying. If the contact angle of the drop is less than 90°, the smallest particles are transported and deposited at the outer part of the ring.[42,43] This effect was also demonstrated to be efficient for the separation of proteins, bacteria and cells in a drying drop.[44] In our protein/particle mixtures, the double-ring is associated with the simultaneous deposition of PS particles and BSA molecules. Their sorting in the final deposit is in agreement with the large difference in size between BSA (diameter ~7 nm) and PS particles (~500 nm). In summary, both BSA and negatively charged particles formed rings when mixed together with a sorting occurring according to their respective sizes.

In the case of the cationic PS-AMI particles, the evolution of the patterns was markedly different (Figure 2 *left*, Figure S3). Without BSA, a dark ring of particles was also observed but its interior was darker than that observed for anionic particles (Figure 2, pattern p1). This is explained by the adsorption of cationic PS-AMI particles on the negatively charged glass substrate, in agreement with previous reports.[20] Adding BSA to this system had a dramatic effect on the pattern evolution. The ring thickness progressively decreased while the interior of the drop became darker (Figure 2, patterns p2–p3; Figure S3) indicating the depletion of the ring and the deposition of the particles inside the drop. For [BSA] $\geq$ 10 μM, the particle ring

DOI: 10.1021/jacs.6b04833
J. Am. Chem. Soc. 2016, 138, 11623–11632

completely disappeared and a homogeneous deposit was formed. Interestingly, although the CRE for particles was efficiently suppressed, light gray rings of proteins were also visible for [BSA] ≥ 10 μM. This shows that, although inhibited by BSA for PS-AMI particles, the CRE was still efficient for free BSA molecules in solution. This demonstrates that the suppression of the CRE by the proteins was not due to a modification of the evaporation-induced flow in the drop. In summary, above a threshold concentration (about 10 μM), BSA suppressed the CRE of cationic particles, leading to homogeneous particle deposits surrounded by rings of proteins in excess.

To systematically assess the effect of BSA on the pattern evolution, we performed an automated image analysis to extract the so-called Ring Factor (RF) for a large number of samples. Briefly, this method, which we developed in the past for other types of "coffee-stain" deposits,[24] consisted in establishing a normalized radial intensity profile from each pattern transmission image. RF was then calculated by comparing the respective contributions of particles in the ring and inner regions. With this analysis, RF was in the range 0.5−0.6 for marked ring patterns, decreased when the fraction of particles in the inner region increased, and reached a value around 0 for disk-like deposits. RF was calculated for the three types of particles as a function of BSA concentration between 0 and 10 μM on triplicated samples (Figure 3). Interestingly, this analysis

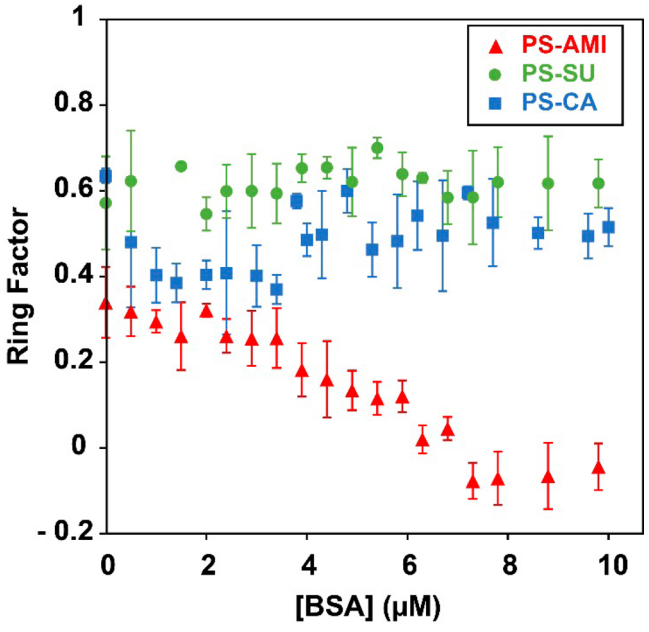

Figure 3. Ring factor (RF) evolution as a function of BSA concentration. RF was calculated by image analysis of the patterns obtained with PS-AMI (red triangles), PS-SU (green disks) and PS-CA (blue squares) particles. Error bars correspond to mean ± sd on triplicates.

showed that, although some sample-to-sample variability was present, general trends in the pattern evolution can be assessed with statistical significance. It also quantitatively confirmed the evolution deduced from simple qualitative observation of the patterns (Figures 2, S1−S3). For anionic particles, all patterns had a characteristic ring signature with RF around 0.5 (RF = 0.55 ± 0,09) regardless of BSA concentration while, for cationic particles, the patterns progressively evolved from a weak ring behavior (RF ≈ 0.3) to homogeneous disks (RF ≈ 0) when BSA increased from 0 to 10 μM.

The different pattern evolution observed for anionic and cationic particles in the presence of a negatively charged protein such as BSA suggests that protein/particle electrostatic interactions may play a role in affecting the CRE of particles. To characterize these interactions, we measured the adsorption isotherms of BSA on PS-CA, PS-SU and PS-AMI (Figure 4A).

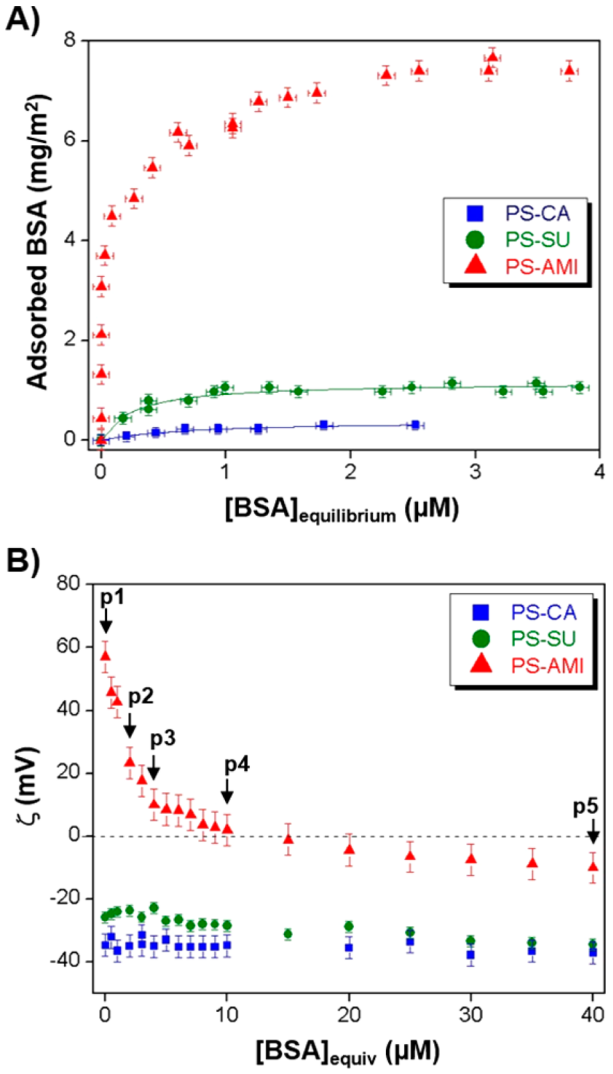

Figure 4. Adsorption behavior of BSA on particles. (A) Adsorption isotherms of BSA on PS-CA (blue squares), PS-SU (green disks) and PS-AMI (red triangles) fitted by the Langmuir model (solid lines). (B) Zeta potential (ζ) of PS-CA (blue squares), PS-SU (green disks) and PS-AMI (red triangles) as a function of equivalent BSA concentration. The arrows indicate the corresponding pattern numbers (p1−p5) shown in Figure 2.

The maximum amount of adsorbed protein m_{ads} was determined by the plateau value of the adsorption isotherm. The adsorption constant K_{ads} was calculated by fitting the experimental data to the Langmuir model, when a good fitting was obtained (Table 1). The use of a reversible adsorption model such as Langmuir isotherm is debated given that protein/particle interaction often leads to virtually irreversible adsorption, due to protein spreading and structural modifications on the surface.[45] However, following Norde and Haynes[46]

DOI: 10.1021/jacs.6b04833
J. Am. Chem. Soc. 2016, 138, 11623−11632

Table 1. Maximum Amount (m_{ads}) and Adsorption Constant (K_{ads}) of BSA on Particles

particles	m_{ads} (mg/m^2)	K_{ads} (L mol^{-1})
PS-CA	0.3 ± 0.1	4.5 × 10^5
PS-SU	1.1 ± 0.1	1.3 × 10^6
PS-AMI	7.5 ± 0.2	–

we believe that the Langmuir model can give a valid thermodynamic description of the first interaction steps of proteins with particles, involving in particular long-range electrostatic interactions, subsequently followed on a longer time scale by protein reorganization.[47,48]

As expected, Figure 4 and Table 1 show a strong adsorption of BSA on cationic particles (PS-AMI) due to favorable electrostatic interactions between the predominant negative charges of the protein and the positive amidine groups. Interestingly, it shows that a significant amount of BSA also adsorbed on negatively charged PS particles, to a rather large extent on PS-SU and to a smaller extent on PS-CA.

The adsorption of BSA on anionic particles can be explained by the fact that the global protein charge is not the most relevant criterion for predicting protein adsorption on particles.[35] Indeed proteins carry a large number of both positively and negatively charged residues. Among 583 residues, BSA is composed of 82 basic residues (Lys, Arg) and 99 acidic residues (Glu, Asp) whose degree of dissociation depends on both pH and their local environment in the protein structure. At pH 6.8, the effective charge of BSA is estimated to be −8.[49] The adsorption of BSA on anionic particles can thus be explained either by favorable electrostatic interactions between some positive residues and the negative moieties on the surface or by hydrophobic interactions with the nongrafted areas of the polystyrene particles. Since the number of grafted groups is much smaller for PS-SU compared to PS-CA particles (0.02 and 0.88 groups/nm^2, respectively, according to manufacturer data), a predominance of hydrophobic interactions with nongrafted areas would explain the higher adsorption constant of BSA on PS-SU than on PS-CA particles (Table 1). BSA adsorption could also be promoted by water displacement and protein rearrangement on the polystyrene surface. Contrary to the situation with PS-SU and PS-CA particles, the adsorption isotherm of BSA on PS-AMI particles deviates from the Langmuir model (Figure 4A), indicating a different adsorption mechanism. The amount of adsorbed BSA on PS-AMI particles is also much larger than usual values for monolayer adsorption on surfaces. If we consider that the minimum surface covered by one BSA molecule (approximated size 9 × 5.5 × 5.5 nm^3) is about 30 nm^2, then the maximum amount of adsorbed BSA at monolayer saturation would be 3.7 mg/m^2. The measured value of 7.5 ± 0.2 mg/m^2 is approximately twice this amount. This simple calculation suggests multilayer adsorption of BSA on PS-AMI particles, at least as dimers. BSA has indeed a tendency to associate into oligomers in solution[50] and can easily establish protein−protein interactions to form dimers on flat surfaces.[51] In summary, BSA adsorbed on both anionic (PS-SU, PS-CA) and cationic (PS-AMI) particles due to a combination of electrostatic and hydrophobic effects but the amount of adsorbed protein was much larger in the case of cationic particles.

The comparison of the deposit patterns (Figure 2) with the adsorption isotherms (Figure 4A, S6) reveals that disk formation is associated with the strong adsorption of BSA on PS-AMI particles. On the contrary, a low level of BSA adsorption on the anionic particles, which also meant that a large excess of protein was free in solution, did not alter particle deposition. Thus, the sole effect of BSA at the air/water interface (modification of the drop surface tension, Figure S5), in the bulk (modification, if any, of the evaporation-driven flow) or the adsorption on the substrate cannot suppress the CRE. The interaction of the protein with particles and a minimum amount of adsorbed protein is thus necessary to obtain a disk pattern. To better understand how protein adsorption can alter particle deposition, we analyzed the evolution of the zeta potential of the particles during protein adsorption (Figure 4B). Adsorption of BSA on PS-AMI particles led to a dramatic decrease of the zeta potential from ζ = 57 ± 5 mV without BSA to ζ = −10 ± 5 mV at 40 μM BSA. Note that no major change of pH was observed upon addition of PS particles or BSA to the solution (Figure S7), showing that protein adsorption is the main determinant of this ζ evolution. Strikingly, charge reversal occurred for a BSA concentration around 10 μM, which is the concentration at which the CRE of PS-AMI particles was suppressed (Figure 2, pattern p4). For lower BSA concentration, particles remained significantly charged (high and positive values of ζ) and the CRE was still present (Figure 2 patterns p1−p3). The suppression of the CRE and the formation of a disk pattern thus corresponded to the neutralization of PS-AMI particles by BSA, in a way reminiscent to the effect of surfactants on oppositely charged particles.[20] By contrast, in the case of anionic particles, no major change of the zeta potential of the particles was observed but a slight decrease was measured, from ζ = −26 ± 2 mV (PS-SU) and ζ = −32 ± 3.5 mV (PS-CA) to ζ = −35 ± 2 mV for both particles when [BSA] increased from 0 to 40 μM, in agreement with a small level of adsorbed BSA on these particles (Figure 4A). Interestingly, for all of these BSA concentrations, the CRE was maintained for both PS-SU and PS-CA particles (Figure 2, patterns p1−p5). Thus, protein adsorption occurred but did not result in charge neutralization and could not suppress the CRE in BSA/PS-SU and BSA/PS-CA systems. In summary, we have found that BSA, a globally anionic protein at neutral pH, affected the CRE mainly by its interactions with particles and not by its behavior at the liquid/air interface. It adsorbed on both anionic and cationic particles but suppressed the CRE only in the case of cationic ones and when the adsorbed amount of protein was sufficient to induce an overall charge neutralization of the particles.

Effect of Porcine Hemoglobin (p-HbA) on the Deposit Patterns of PS Particles. We then investigated the effect of p-HbA, a major blood protein characterized by a tetrameric structure ($\alpha_2\beta_2$) and a global positive charge in pure water (IEP pH ∼ 7.0), on the deposit patterns of the same cationic and anionic PS particles (Figures 5, S8−S10). First, in the case of cationic particles (PS-AMI), the effect of p-HbA on the deposit patterns was strikingly similar to that of BSA with negatively charged particles. The addition of p-HbA, regardless of its concentration, did not significantly affect the formation of the particle ring (Figure 5, *left* and Figures S10−S11), although a progressive decrease of the amount of particles inside the ring was observed with an increase in [p-HbA], which is attributed to the adsorption of protein on the glass substrate preventing the Coulomb particle-substrate attraction.[20,52] The gray ring of proteins surrounding the black ring of particles was also observed, in agreement with the p-HbA ring formation in the absence of particles (Figure S4). We detected that a small

DOI: 10.1021/jacs.6b04833
J. Am. Chem. Soc. 2016, 138, 11623−11632

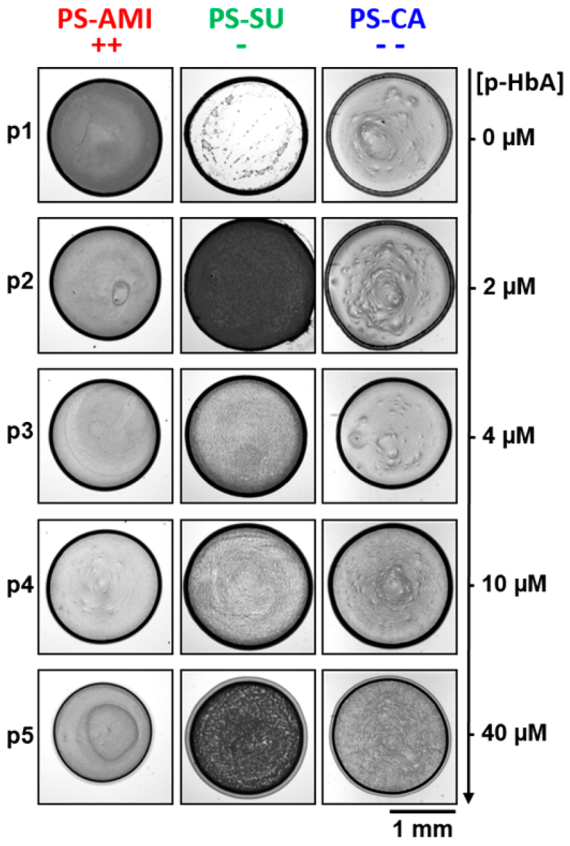

Figure 5. Effect of p-HbA on deposit morphologies. Representative brightfield microscope images of the deposit patterns obtained with PS-AMI (left), PS-SU (middle), and PS-CA (right) as a function of p-HbA concentration. The pattern names, p1−p5, which refer to each p-HbA concentration, are those used in Figure 6B.

amount of p-HbA could adsorb on PS-AMI (Figure 6A, Table 2), to an extent similar to BSA on anionic particles (Figure 4A, Table 1), but p-HbA did not follow a regular Langmuir adsorption behavior. The adsorption isotherm of p-HbA on PS-AMI followed an S-shape curve that could not be fitted by any of the classical two-parameter adsorption models tested (Langmuir, Freundlich, Jovanovic, Temkin-Pyzhev, Dubinin-Radushkevic and Halsey models).[48] Because HbA is a tetrameric protein, we hypothesized that association or dissociation of subunits during adsorption could account for this concentration-dependent adsorption behavior. To check this hypothesis, we measured the adsorption isotherm of myoglobin (Mb), a monomeric heme protein with a similar secondary structure and global charge (IEP pH ∼ 7.4) (Figure S12). The amount of adsorbed protein on PS-AMI was identical (m_{ads} = 0.6 mg/m^2) but the adsorption isotherm of Mb followed a classical Langmuir model. Thus, Mb and p-HbA led to similar amount of adsorbed protein on the particle surface but the adsorption process is different. It thus suggests that monomeric and oligomeric proteins with similar charge do not follow the same adsorption pathway on PS-AMI particles. The highly positive zeta potential of PS-AMI particles (ζ = 57 ± 5 mV in the absence of proteins) did not significantly change from 0 to 10 μM p-HbA (Figure 6B) corresponding to the plateau value of the adsorption isotherm (Figure S13). It then slightly decreased at higher protein concentration suggesting that additional p-HbA adsorbed either by protein/surface or protein/protein interactions. Overall, the particles remained

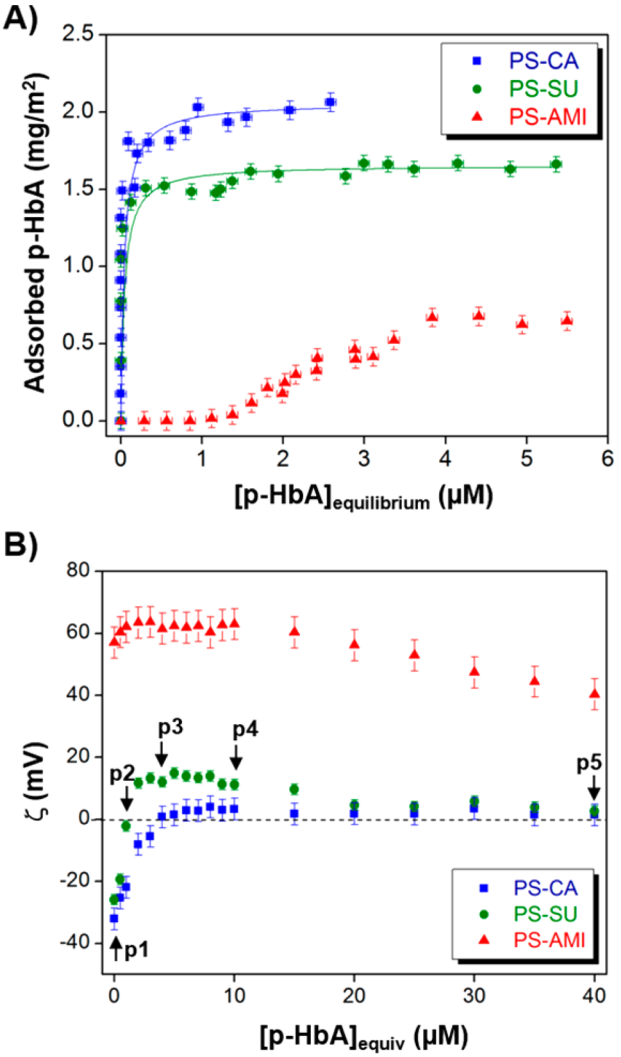

Figure 6. Adsorption behavior of p-HbA on particles. (A) Adsorption isotherms of p-HbA on PS-CA (blue squares), PS-SU (green disks) and PS-AMI (red triangles) fitted by the Langmuir model (solid line). (B) Zeta potential (ζ) of PS-CA (blue squares), PS-SU (green disks) and PS-AMI (red triangles) as a function of equivalent p-HbA concentration. The arrows indicate the corresponding pattern numbers (p1−p5) shown in Figure 5.

Table 2. Maximum Amount (m_{ads}) and Adsorption Constant (K_{ads}) of p-HbA on Particles

particles	m_{ads} (mg/m^2)	K_{ads} (L mol^{-1})
PS-CA	2.0 ± 0.06	8.2 × 10^6
PS-SU	1.65 ± 0.05	7.5 × 10^6
PS-AMI	0.65 ± 0.06	–

highly positive (ζ = 40 ± 5 mV at 40 μM). In summary, p-HbA adsorbed on cationic particles to a limited extent but did not affect the CRE of particles because the latter remained highly charged regardless of added protein concentration.

Conversely, p-HbA strongly adsorbed on negatively charged particles (Figure 6A, Table 2). The light gray protein ring pattern surrounding the particle deposit was also observed for [p-HbA] ≥ 10 μM. However, p-HbA had a strong influence on the particle pattern formation only in the case of PS-SU (Figure 5 *middle* and Figure S8). In this case, the addition of p-HbA resulted in the progressive formation of a disk by depletion of

DOI: 10.1021/jacs.6b04833
J. Am. Chem. Soc. 2016, 138, 11623−11632

the ring and accumulation of PS-SU particles inside the drop, leading to particularly homogeneous particle deposits for 0.9 ≤ [p-HbA] ≤ 2 μM (Figure 5, pattern p2). From 2.4 to 15 μM, the interior of the drop was depleted and the black particle ring was formed again (Figure 5, patterns p3 and p4, Figure S8). This ring-disk-ring evolution was confirmed by the ring factor analysis which showed a minimum at intermediate [p-HbA] (Figure S11). With a further increase in p-HbA, particles were deposited again inside the drop leading to mixed disk/ring patterns with an increasing amount of particles in the disk region (Figure 5, pattern p5). This pattern evolution correlated remarkably well with the ζ evolution of PS-SU particles as a function of [p-HbA] (Figure 6B). For instance, p-HbA adsorption led to charge neutralization of PS-SU particles at about [p-HbA] = 1.5 μM (ζ = −2.1 ± 1.7 mV), which corresponded exactly to the formation of the most homogeneous disk (pattern p2). Further protein adsorption resulted in charge reversal and positive charging of PS-SU particles from 2 to 15 μM p-HbA, associated with the formation of ring patterns again, such as p3 (ζ = 12.1 ± 1.7 mV) and p4 (ζ = 11.2 ± 1.7 mV). With a further increase in protein concentration, ζ became nearly neutral again, accompanied by the formation of mixed disk/ring patterns (e.g., p5). All these results confirm that the protein adsorption-induced charge neutralization of particles, rather than the simple extent of protein adsorption, is a key determinant of the suppression of the CRE in protein/particle mixtures.

Surprisingly, a different behavior was observed for PS-CA particles where p-HbA adsorption resulted in complete particle charge neutralization without formation of a homogeneous particle deposit. For instance, the CRE was maintained at [p-HbA] = 4 μM (RF = 0.50 ± 0.01) despite the neutralization of the particles (ζ = 0.8 ± 3.5 mV) (pattern p3). For larger protein concentrations (4 ≤ [p-HbA] ≤ 40 μM), the particles remained almost neutral with no modification of the ring pattern (patterns p4−p5), hence impeding the generalization of the straightforward relationship between particle charge neutralization and disk formation in protein/particle mixtures. This implies that other mechanisms, such as a reorganization of the protein at the surface of the particles or a shielding of the particle charged moieties, should be taken into account in the relationship between particle-protein interaction and pattern morphological properties.

Detection of a Single-Point Mutation by Pattern Analysis. Our results suggested that the pattern formation was very sensitive to the interaction between proteins and particles, especially in the case of p-HbA. We thus hypothesized that a single-point mutation present in a protein, by changing the interaction of the proteins with particles in solution, could be detected by pattern analysis of drying drops. To check this hypothesis, we compared the effect of native human hemoglobin (h-HbA) to sickle cell hemoglobin (h-HbS) in the way it affects the CRE of PS-SU particles, for which a marked suppression of the CRE by p-HbA particles was observed. h-HbS carries a single mutation Glu → Val (β6) responsible for sickle cell anemia due to h-HbS polymerization in its deoxygenated form.[53] Both proteins were in the oxygenated form meaning that h-HbS was not in its polymerized form and had the same structure as h-HbA. We anticipated that the replacement of a single charged glutamic acid with a hydrophobic valine residue could result in a detectable change in the pattern formation of PS-SU particles.

We analyzed the deposit patterns and the zeta potentials of PS-SU particles with human hemoglobin in both native (h-HbA) and mutant (h-HbS) forms, at protein concentrations of 1 μM, 1.5 μM and 15 μM (Figure 7). At 1 μM, adsorption of h-

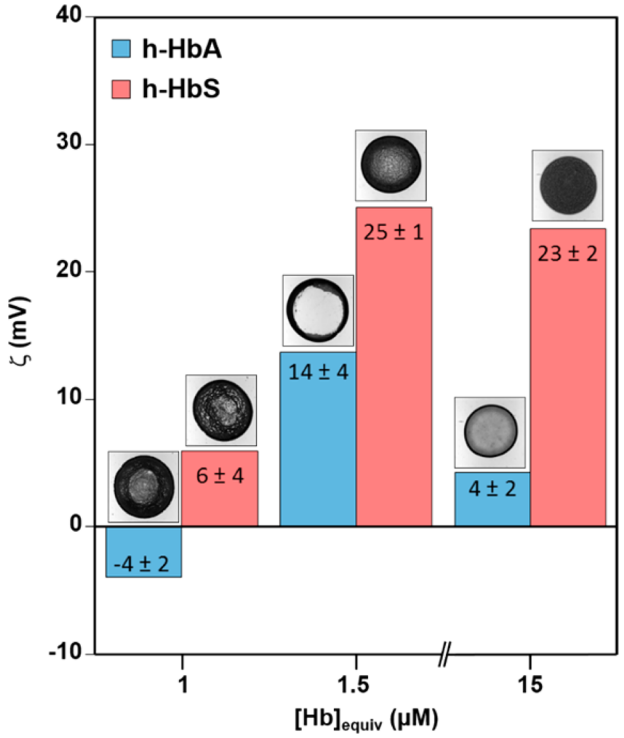

Figure 7. h-HbA and its pathogenic mutant h-HbS interact differently with PS-SU particles thus inducing different deposit morphologies. Zeta-potential (ζ) of PS-SU particles as a function of equivalent protein concentration ($[Hb]_{equiv}$) for both the native form (h-HbA) and the mutant form (h-HbS) of human hemoglobin. For each condition, the corresponding patterns after drop drying (top) and the ζ values (mean ± sd) are indicated. Each image is 2.2 mm × 2.2 mm.

HbA and h-HbS on PS-SU led to particle charge neutralization and to the formation of a more homogeneous deposit with both proteins compared to the ring-shaped patterns in the absence of proteins (patterns p1 in Figures 2, 5). At 1.5 μM, an increase of the zeta potential was observed for h-HbA accompanied by the formation of a ring pattern. At a higher h-HbA concentration (15 μM), we observed a decrease of the zeta potential and a ring pattern with a larger amount of particles inside the ring. h-HbA thus behaved in a way similar to p-HbA, both in terms of protein/particle interactions and deposit pattern formation.

A very different behavior was observed for h-HbS. At 1.5 μM, a larger increase of the zeta potential was measured (ζ = 25 ± 1 mV). This effect can be rationalized by the higher isoelectric point of h-HbS (IEP pH = 7.2) compared to h-HbA (IEP pH = 7.0).[54] Surprisingly, this positive charge did not prevent the deposition of a large amount of particles inside the drop. At 15 μM, the zeta potential of the particles remained high and a perfect disk pattern was formed. Thus, two different behaviors should be considered as a function of h-HbS concentration. At [h-HbS] = 1 μM, protein adsorption led to particle charge neutralization and suppression of the coffee-ring effect, as observed for BSA, p-HbA and native h-HbA. In contrast, at [h-HbS] = 1.5 μM and 15 μM, particles were overcharged by the adsorbed proteins but the final deposit was a disk. Since the

DOI: 10.1021/jacs.6b04833
J. Am. Chem. Soc. 2016, 138, 11623−11632

main difference between h-HbA and h-HbS is the replacement of a charged glutamic acid with the hydrophobic valine residue, we can hypothesize that the specific effects observed with h-HbS are due to conformational modifications on the particle surface and/or additional exposure of hydrophobic regions.

Because the pattern formation was found to be very sensitive to the hydrophobicity change of a single exposed residue in h-HbA, this method seemed to be applicable as a robust cost-effective tool to detect pathogenic point-mutations in some proteins. To emphasize the importance of the particles, we analyzed the patterns of h-HbA and h-HbS in the absence and presence of PS-SU particles (Figure 8). Without particles, both

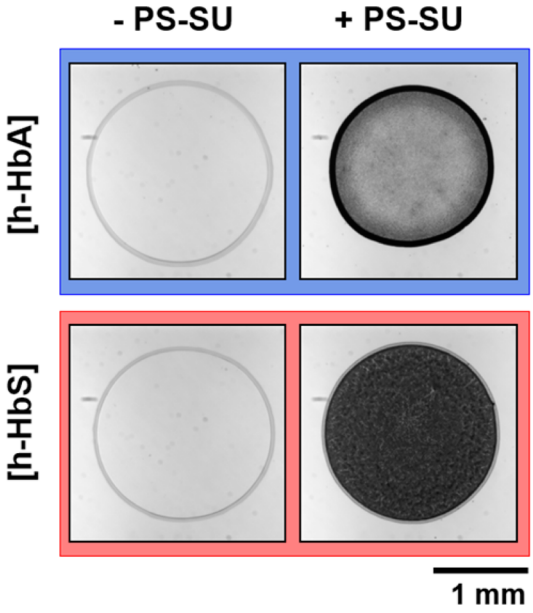

Figure 8. A single-point mutation in h-HbA results in a dramatic change of the deposit morphology. Representative brightfield microscope images of the deposit patterns obtained with 15 μM of human hemoglobin, either in its native form (h-HBA, top) or in its pathogenic mutant form (h-HbS, bottom) in the absence (left) and presence (right) of PS-SU particles (2 mg/mL).

proteins formed the usual light gray rings, which could not be distinguished from each other. By contrast, in the presence of particles, only the pathogenic mutant h-HbS led to a homogeneous disk pattern, which was easily distinguishable from the pattern formed with native h-HbA where the majority of particles accumulated at the ring position. To quantify the robustness of this detection, we systematically measured the ring factor by independent preparation of several solutions of identical composition (n, number of prepared solutions) and several drop depositions for each solution (p, total number of analyzed patterns). We found RF = 0.46 ± 0.02 (n = 5, p = 17) and RF = 0.16 ± 0.10 (n = 7, p = 22) for h-HbA and h-HbS, respectively, showing that detection of the specific formation of a ring versus disk pattern can be used as a robust diagnostic tool to discriminate beween native h-HbA (ring, RF > 0.4) and its pathogenic mutant h-HbS (disk, RF < 0.2).

Probing Protein/Particle Interactions by the CRE. Finally, based on the different results we have obtained, we discuss here whether observing the CRE in drying drops could be used as a generic tool to probe interactions between proteins and particles. We analyzed several types of protein/particle mixtures and found that protein adsorption led to the suppression of the coffee-ring effect primarily when it was associated with the particle charge neutralization (Figure 9,

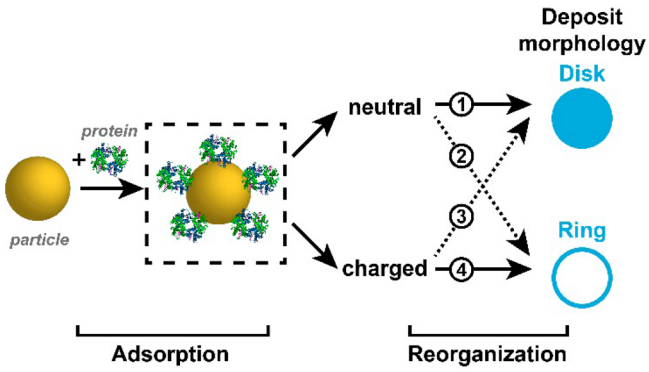

Figure 9. Probing protein adsorption and reorganization on particles by pattern analysis of drying drops. The adsorption behavior of proteins on particles results in an overall modification of the particle charge that primarily determines the deposit morphology (paths 1 and 4). Exposure of charged (path 2) or hydrophobic (path 3) moieties upon reorganization on particle surface can invert this effect. Analyzing the deposit morphology is thus a way to probe the adsorption and reorganization behavior of proteins on particle surfaces.

path 1) while a marked ring pattern was observed with globally highly charged particles (Figure 9, path 4). This mechanism was relevant for BSA adsorption on PS-AMI, PS-SU and PS-CA particles and for both p-HbA and h-HbA on PS-SU particles. This behavior is in remarkable agreement with what has been observed in surfactant/particle systems with surfactant concentrations below the critical micellar concentration (CMC).[20] The CRE was shown to be suppressed only in the case of oppositely charged surfactant, and for a specific window of concentrations for which particles were neutralized by an adsorbed layer of surfactants. This neutralization led to the trapping of particles at the liquid/gas (LG) interface which prevented the particles from being transported to the drop edge by the evaporation-driven flow. A similar trapping phenomenon was observed in the protein/particle systems we have investigated here. Microscopic observation of the LG interface of the drops during drying showed that the formation of a network of particles trapped at the LG interface led to rather homogeneous deposition of particles in the center of the deposit while the absence of particle trapping led to the marked ring pattern. Note that when particles adsorbed at the LG interface during evaporation, they also formed small aggregates at the LG interface indicating that trapping and aggregation can occur at the same time. We can assume that either particles started forming small aggregates in the bulk that were swept by the moving air/water interface during drying,[20] or that hydrophobic particles were first trapped at the air/water interface where they associated to form a 2D network.

However, we observed that the simple particle charge neutralization by protein adsorption cannot always account for the suppression of the CRE, which distinguishes proteins from ordinary surfactants. This mechanism proved to be counteracted by specific effects in the case of p-HbA adsorption on PS-CA particles and mutant h-HbS interaction with PS-SU particles. Interestingly, the CRE was not suppressed in the first case, although PS-CA were neutralized by p-HbA adsorption (Figure 9, path 2), whereas it was efficiently suppressed in the

DOI: 10.1021/jacs.6b04833
J. Am. Chem. Soc. 2016, 138, 11623−11632

second case, though PS-SU particles were not neutralized by h-HbS adsorption (Figure 9, path 3).

The above findings suggest that p-HbA adsorption on PS-CA particles could not drive particle adsorption at the air/water interface though particles were overall neutrally charged. This could be explained by specific structural modifications of adsorbed p-HbA on PS-CA preventing particle adsorption and aggregation. Indeed it was reported by Barbosa and co-workers that partially unfolded BSA can lead to strong repulsive protein−protein interaction in solution for a given concentration due to larger exposure of charges.[50] It was also stressed out by Chen and co-workers that BSA can adopt a more "hydrophilic" or "hydrophobic" conformation when adsorbed at different interfaces.[55] If a similar process occurs at the particle surface, then specific p-HbA conformation on PS-CA particles could possibly account for repulsive interactions between particles independently of their global charge.

On the contrary, h-HbS adsorption could favor particle aggregation or particle adsorption at the air/water interface by exposure of hydrophobic regions of the adsorbed protein on PS-SU particles. Previous studies of the behavior of mutant hemoglobins at the air/water interface revealed that h-HbS is more surface active than h-HbA, as evidenced by a faster adsorption and a larger occupied area per molecule meaning that h-HbA and h-HbS have different structures at the interface.[53] The higher surface activity could also enhance protein-mediated interactions of charged particles at the air/water interface.

All these results show that protein structural modifications at the particle surface play a key role affecting the CRE in protein/particle mixtures, thus making possible to probe such reorganizations by simple pattern analysis. This analysis was done qualitatively by visual inspection or, in a more quantitative manner, by computation of a ring factor from image analysis. An illustration of this probing capability was provided by the dramatic change of the deposit morphology induced by a single-point mutation in human hemoglobin.

CONCLUSION

We systematically investigated the effect of various proteins on the deposit patterns of sessile drops containing polystyrene particles with different surface functionalizations. Our main result is that, although each protein led to some specific behavior, general rules could be drawn. Particles rendered hydrophobic by protein adsorption, either by neutralization of their charge or specific exposure of hydrophobic regions, tended to accumulate at the LG interface and formed a rather homogeneous, disk-like deposit after drop drying. In contrast, when particles, after protein adsorption, did not have affinity for the LG interface (highly charged), they accumulated at the drop edge, leaving a coffee-ring-like deposit after drop drying. Interestingly, this principle was applied to discriminate, via simple inspection of the deposit pattern, between a healthy and a pathogenic form of human hemoglobin, which differed by only a single amino acid. The interest of this work is thus multifold. First, it unveils a new and robust way to suppress the coffee-ring effect (CRE). Indeed, adding the right amount of a proper protein to a colloidal suspension was shown to be an efficient way to create homogeneous deposits of particles that otherwise would form a ring. Second, simple observation of the deposit patterns of protein/particle suspension systems appears as a straightforward manner to quickly get qualitative information on how proteins interact with particles as well as the extent of their adsorption and reorganization on the particle surface. Hence, using the CRE to probe these interactions can be exploited in different ways. First, it can be exploited to distinguish between a native and a mutant form of a specific protein, especially when mutation leads to hydrophobic residue exposure, as presented in this paper with the robust discrimination between native and sickle cell human hemoglobin. Second this could be useful to investigate protein reorganization and charge modification after adsorption on particles in the context of nanotoxicology and nanomedicine, for instance to screen in a rapid and low-resource way a large number of proteins and nanoparticles. These two new types of screening assays could reach high-throughput capabilities by benefiting from the development of automatic pattern recognition softwares.[56] Overall, we have shown how the CRE translates various types of molecular interactions between particles and proteins into easily distinguishable macroscopic patterns, thus providing valuable insights for the development of current and future cost-effective diagnostic tools.

ASSOCIATED CONTENT

Supporting Information

The Supporting Information is available free of charge on the ACS Publications website at DOI: 10.1021/jacs.6b04833.

Additional deposit patterns; deposit patterns of pure protein solutions; surface tension measurement; pH measurement; adsorption isotherm as a function of the initial protein concentration; adsorption isotherm of myoglobin; Ring Factor analysis of deposit patterns with p-HbA. (PDF)

AUTHOR INFORMATION

Corresponding Author

*damien.baigl@ens.fr

Present Address

⊥Centre for BioNano Interactions, School of Chemistry, University College Dublin, Belfield, Dublin 4, Ireland.

Notes

The authors declare no competing financial interest.

ACKNOWLEDGMENTS

This work was supported by the European Research Council (ERC) [European Community's Seventh Framework Programme (FP7/2007−2013)/ERC Grant agreement no. 258782)] and the Mairie de Paris [Emergence(s) 2012]. MA acknowledges funding from the European Commission (FP7-PEOPLE-2013-IEF/Project 624806 "DIOPTRA").

REFERENCES

(1) Deegan, R. D.; Bakajin, O.; Dupont, T. F.; Huber, G.; Nagel, S. R.; Witten, T. A. *Nature* **1997**, *389*, 827−829.

(2) Sempels, W.; De Dier, R.; Mizuno, H.; Hofkens, J.; Vermant, J. *Nat. Commun.* **2013**, *4*, 1757.

(3) Thokchom, A. K.; Swaminathan, R.; Singh, A. *Langmuir* **2014**, *30*, 12144−12153.

(4) Gebhardt, R.; Teulon, J.-M.; Pellequer, J.-L.; Burghammer, M.; Colletier, J.-P.; Riekel, C. *Soft Matter* **2014**, *10*, 5458−5462.

(5) Gorr, H. M.; Zueger, J. M.; Barnard, J. A. *Langmuir* **2012**, *28*, 4039−4042.

(6) Gorr, H. M.; Zueger, J. M.; McAdams, D. R.; Barnard, J. A. *Colloids Surf., B* **2013**, *103*, 59−66.

(7) Sobac, B.; Brutin, D. *Phys. Rev. E* **2011**, *84*, 1−5.

(8) Park, J.; Moon, J. *Langmuir* **2006**, *22*, 3506−3513.

(9) Blossey, R.; Bosio, A. *Langmuir* **2002**, *18*, 2952−2954.
(10) Dugas, V.; Broutin, J.; Souteyrand, E. *Langmuir* **2005**, *21*, 9130−9136.
(11) Deng, Y.; Zhu, X.-Y.; Kienlen, T.; Guo, A. *J. Am. Chem. Soc.* **2006**, *128*, 2768−2769.
(12) Mujawar, L. M.; Kuerten, J. G. M.; Siregar, D. P.; van Amerongen, A.; Norde, W. *RSC Adv.* **2014**, *4*, 19380−19388.
(13) Keskin, S.; Culha, M. *Analyst* **2012**, *137*, 2651−2657.
(14) Roth, E. A.; Xu, T.; Das, M.; Gregory, C.; Hickman, J. J.; Boland, T. *Biomaterials* **2004**, *25*, 3707−3715.
(15) Yunker, P. J.; Still, T.; Lohr, M. A.; Yodh, A. G. *Nature* **2011**, *476*, 308−311.
(16) Larson, R. G. *Angew. Chem., Int. Ed.* **2012**, *51*, 2546−2548.
(17) Larson, R. G. *AIChE J.* **2014**, *60*, 1538−1571.
(18) Anyfantakis, M.; Baigl, D. *ChemPhysChem* **2015**, *16*, 2726−2734.
(19) Still, T.; Yunker, P. J.; Yodh, A. G. *Langmuir* **2012**, *28*, 4984−4988.
(20) Anyfantakis, M.; Geng, Z.; Morel, M.; Rudiuk, S.; Baigl, D. *Langmuir* **2015**, *31*, 4113−4120.
(21) Cui, L.; Zhang, J.; Zhang, X.; Huang, L.; Wang, Z.; Li, Y.; Gao, H.; Zhu, S.; Wang, T.; Yang, B. *ACS Appl. Mater. Interfaces* **2012**, *4*, 2775−2780.
(22) Talbot, E. L.; Yang, L.; Berson, A.; Bain, C. D. *ACS Appl. Mater. Interfaces* **2014**, *6*, 9572−9583.
(23) Mampallil, D.; Eral, H. B.; van den Ende, D.; Mugele, F. *Soft Matter* **2012**, *8*, 10614−10617.
(24) Anyfantakis, M.; Baigl, D. *Angew. Chem., Int. Ed.* **2014**, *53*, 14077−14081.
(25) Varanakkottu, S. N.; Anyfantakis, M.; Morel, M.; Rudiuk, S.; Baigl, D. *Nano Lett.* **2016**, *16*, 644−650.
(26) Choi, S.; Stassi, S.; Pisano, A. P.; Zohdi, T. I. *Langmuir* **2010**, *26*, 11690−11698.
(27) Zhang, Z.; Zhang, X.; Xin, Z.; Deng, M.; Wen, Y.; Song, Y. *Adv. Mater.* **2013**, *25*, 6714−6718.
(28) Wen, J. T.; Ho, C.-M.; Lillehoj, P. B. *Langmuir* **2013**, *29*, 8440−8446.
(29) Gulka, C. P.; Swartz, J. D.; Trantum, J. R.; Davis, K. M.; Peak, C. M.; Denton, A. J.; Haselton, F. R.; Wright, D. W. *ACS Appl. Mater. Interfaces* **2014**, *6*, 6257−6263.
(30) Trantum, J. R.; Wright, D. W.; Haselton, F. R. *Langmuir* **2012**, *28*, 2187−2193.
(31) Hurth, C.; Bhardwaj, R.; Andalib, S.; Frankiewicz, C.; Dobos, A.; Attinger, D.; Zenhausern, F. *Chem. Eng. Sci.* **2015**, *137*, 398−403.
(32) Trantum, J. R.; Baglia, M. L.; Eagleton, Z. E.; Mernaugh, R. L.; Haselton, F. R. *Lab Chip* **2014**, *14*, 315−324.
(33) Li, Y.; Zhao, Z.; Lam, M. L.; Liu, W.; Yeung, P. P.; Chieng, C.-C.; Chen, T.-H. *Sens. Actuators, B* **2015**, *206*, 56−64.
(34) Norde, W. *Colloids Surf., B* **2008**, *61*, 1−9.
(35) Mathé, C.; Devineau, S.; Aude, J.-C.; Lagniel, G.; Chédin, S.; Legros, V.; Mathon, M.-H.; Renault, J.-P.; Pin, S.; Boulard, Y.; Labarre, J. *PLoS One* **2013**, *8*, e81346.
(36) Yuan, Y.; Oberholzer, M. R.; Lenhoff, A. M. *Colloids Surf., A* **2000**, *165*, 125−141.
(37) Perutz, M. F. *J. Cryst. Growth* **1968**, *2*, 54−56.
(38) Antonini, E.; Brunori, M. *Hemoglobin and Myoglobin in Their Interactions with Ligands*; North Holland Pub. Co.: Amsterdam, 1971.
(39) Banerjee, R.; Alpert, Y.; Leterrier, F.; Williams, R. J. *Biochemistry* **1969**, *8*, 2862−2867.
(40) El Antri, S.; Sire, O.; Alpert, B. *Eur. J. Biochem.* **1990**, *191*, 163−168.
(41) Sett, A.; Bag, S.; Dasgupta, S.; DasGupta, S. *Int. J. Biol. Macromol.* **2015**, *79*, 344−352.
(42) Monteux, C.; Lequeux, F. *Langmuir* **2011**, *27*, 2917−2922.
(43) Noguera-Marín, D.; Moraila-Martínez, C. L.; Cabrerizo-Vílchez, M. A.; Rodríguez-Valverde, M. A. *Langmuir* **2015**, *31*, 6632−6638.
(44) Wong, T. S.; Chen, T. H.; Shen, X.; Ho, C. M. *Anal. Chem.* **2011**, *83*, 1871−1873.
(45) Latour, R. A. *J. Biomed. Mater. Res., Part A* **2015**, *103*, 949−958.
(46) Norde, W.; Haynes, C. A. *ACS Symposium Series*; American Chemical Society: Washington D.C., 1995; Vol. *602*, pp 26−40.
(47) Kondo, A.; Fukuda, H. *J. Colloid Interface Sci.* **1998**, *198*, 34−41.
(48) Devineau, S.; Zanotti, J.; Loupiac, C.; Zargarian, L.; Neiers, F.; Pin, S.; Renault, J. P. *Langmuir* **2013**, *29*, 13465−13472.
(49) Böhme, U.; Scheler, U. *Chem. Phys. Lett.* **2007**, *435*, 342−345.
(50) Barbosa, L. R. S.; Ortore, M. G.; Spinozzi, F.; Mariani, P.; Bernstorff, S.; Itri, R. *Biophys. J.* **2010**, *98*, 147−157.
(51) Rezwan, K.; Meier, L. P.; Rezwan, M.; Vörös, J.; Textor, M.; Gauckler, L. J. *Langmuir* **2004**, *20*, 10055−10061.
(52) Bhardwaj, R.; Fang, X. H.; Somasundaran, P.; Attinger, D. *Langmuir* **2010**, *26*, 7833−7842.
(53) Elbaum, D.; Harrington, J.; Roth, E. F.; Nagel, R. L. *Biochim. Biophys. Acta, Protein Struct.* **1976**, *427*, 57−69.
(54) Hempe, J. M.; Craver, R. D. *Electrophoresis* **2000**, *21*, 743−748.
(55) Wang, J.; Buck, S. M.; Even, M. A.; Chen, Z. *J. Am. Chem. Soc.* **2002**, *124*, 13302−13305.
(56) Kim, N.; Li, Z.; Hurth, C.; Zenhausern, F.; Chang, S.-F.; Attinger, D. *Anal. Methods* **2012**, *4*, 50−57.

DOI: 10.1021/jacs.6b04833
J. Am. Chem. Soc. 2016, 138, 11623−11632